Fractional Order Adaptive Fixed-Time Sliding Mode Controller for Synchronization of Fractional Order Chaotic Permanent Magnet Synchronous Motors

Ozhan Bingol

Abstract—This study develops a novel fractional-order adaptive fixed-time sliding mode controller for achieving chaotic synchronization in fractional-order Permanent Magnet Synchronous Motors (PMSMs). PMSMs, widely used in electric vehicles, robotics, and renewable energy systems, are prone to chaotic behavior under parameter variations and external disturbances, which can degrade performance and stability. Existing control strategies often face limitations such as chattering, sensitivity to uncertainties, and dependence on initial conditions. The proposed controller integrates fractional calculus to capture the memory effects inherent in PMSM dynamics, combined with a fixed-time stability framework that guarantees convergence within a fixed time, independent of initial conditions. An adaptive mechanism further enhances the controller's robustness by dynamically tuning parameters to counteract sensor noises, external disturbances, and parameter variations. Simulation results demonstrate the superiority of the proposed controller over existing methods, showcasing faster convergence, improved stability, and reduced chattering. This controller offers a promising solution for chaos suppression and synchronization in PMSMs, paving the way for more reliable and efficient applications in dynamic and uncertain environments.

Index Terms—Fixed-time stability, chaotic synchronization, fractional-order sliding mode, adaptive control.

I. INTRODUCTION

PMSM has emerged as a critical component in modern engineering applications due to its superior performance characteristics, such as high efficiency, power density, and precise torque control [1]. These attributes make PMSMs highly desirable in applications where energy savings, compact designs, and accurate motion control are of paramount importance. As a result, PMSMs are widely integrated across multiple industries, including robotics, where they enable precise movements and automation [2], electric vehicles (EVs), where their high efficiency extends battery life [3], aerospace, where their reliability supports advanced propulsion and actuation systems [4], and renewable energy systems, such as wind turbines, where their robustness ensures stable power generation under varying environmental conditions [5]. However, under certain operating conditions, such as parameter variations, external disturbances, or high-speed regimes, PMSMs can exhibit chaotic behavior [6]. This chaotic response, characterized

by irregular and unpredictable oscillations, can significantly degrade the system's performance, leading to instability, increased energy consumption, and even mechanical failures. To ensure reliable and stable operation, effective control strategies are essential to mitigate chaos and maintain synchronization in PMSM systems.

Over the years, several control techniques have been proposed to address the challenges of chaos control and synchronization in PMSM. Classical approaches include Lyapunov exponent control [7], adaptive robust backstepping [8], nonlinear feedback control [9], and neural network control [10] methods. However, these approaches often suffer from significant limitations. Sensitivity to initial conditions, slow convergence rates, and an inability to capture the memory effects inherent to PMSM dynamics reduce their effectiveness in real-world applications. These challenges motivate the development of advanced control techniques capable of achieving robust performance under diverse and uncertain operating conditions.

Fractional calculus, an extension of traditional calculus, deals with derivatives and integrals of non-integer orders [11]. In recent years, fractional calculus has gained significant attention in control theory due to its ability to model memory and hereditary properties of dynamic systems more accurately [12]. This characteristic makes fractional-order controllers highly suitable for applications involving complex systems, such as PMSMs, where the dynamics are inherently nonlinear and time-varying. Compared to conventional integer-order controllers, fractional-order controllers provide more degrees of freedom, allowing for better tuning of control parameters and improved dynamic response. After fractional order model of PMSM is derived [13], some control strategies have been applied to fractional PMSM systems. A nonlinear state observer-based control strategy for the projective synchronization of a fractional-order chaotic model is derived in [14]. An observer-based command-filtered adaptive neural network tracking control for a fractional-order chaotic PMSM system, considering immeasurable states, parameter uncertainties, and external load disturbances is developed in [1]. An energy feedback controller is proposed in [15], for fractional-order chaotic complex PMSM system.

However, the aforementioned controllers can only ensure asymptotic stability or, at best, exponential stability of the closed-loop system. In contrast, finite-time control guarantees that the synchronization errors converge to zero or to small residual sets around zero within a finite time. A finite-time

Özhan BİNGÖL is with the Department of Electrical and Electronic Engineering, Faculty of Engineering and Natural Sciences, Gumushane University, Gumushane, 29100 TURKIYE e-mail: ozhan.bingol@gumushane.edu.tr

adaptive neural network position tracking control method using command-filtered backstepping is presented in [16]. A finite-time terminal sliding mode control approach based on recurrent neural networks is proposed for fractional-order chaotic systems subject to Gaussian white noise disturbances in [17]. Although finite-time control provides a way to calculate the settling time, this time is highly dependent on the system's initial conditions, diminishing its practical value to some extent. To address this limitation, the concept of fixed-time control was proposed [18]. Fixed-time control can be considered a specialized form of finite-time control, where the settling time is bounded, and the upper limit of this settling time is independent of the initial states of the system. Particularly in recent years, control approaches have been implemented that yield successful results in the control and synchronization of various chaotic systems through the application of fixed-time control methods [19]–[24]. Such studies have shown the effectiveness of the fixed-time approach in controlling and synchronizing chaotic systems. However, achieving fixed-time synchronization of chaotic fractional PMSMs remains an open problem, meriting further investigation.

Fractional-order systems have gained considerable attention in control theory due to their ability to accurately model the dynamics of nonlinear and time-varying systems. Similarly, fixed-time control has emerged as a robust solution for chaotic systems, offering predictable performance by guaranteeing bounded convergence times. By combining these two paradigms, this study presents a novel control framework that addresses critical gaps in the suppression and synchronization of chaotic dynamics in PMSMs.

In light of the above observations, this study proposes a fractional-order adaptive fixed-time sliding mode controller to overcome these challenges. The novelty of the proposed method lies in its integration of fractional calculus with fixed-time control theory. Fractional calculus enables the controller to account for memory effects and hereditary properties, which are intrinsic to many dynamic systems, including PMSMs. Unlike integer-order methods, this approach provides additional flexibility and precision in modeling complex system behaviors. Fixed-time stability ensures that system convergence occurs within a fixed time, regardless of initial conditions, while the adaptive mechanism dynamically tunes control parameters to compensate for sensor noises, parameter uncertainties, external disturbances, and varying load conditions. Additionally, the synergistic combination of sliding mode control, adaptive control, and fractional-order control significantly enhances the robustness, adaptability, and overall stability of the control system. This integrated framework effectively addresses the challenges presented by chaotic dynamics and varying operational conditions, ensuring reliable performance across a diverse range of scenarios.

The remainder of this paper is structured as follows. Section (II) introduces the mathematical preliminaries and problem formulation for fractional-order PMSM dynamics. Section (III) presents the design of the proposed fractional-order adaptive fixed-time sliding mode controller. Section (IV) evaluates the controller's performance through extensive simulations, demonstrating its advantages in terms of faster convergence, reduced chattering, and enhanced robustness. Finally, Section (V) concludes the study with a discussion of the findings, limitations, and potential future research directions.

II. PRELIMINARIES AND PROBLEM FORMULATION

This section provides essential lemmas required for the formulation of the proposed control scheme. Furthermore, it introduces the fundamental principles of fractional calculus. Lastly, the fractional-order dynamics of the PMSM system are presented.

A. Preliminaries

Lemma 1. *([18]) Assume a nonlinear system $\dot{x} = f(x, u)$, if a positive definitive Lyapunov function $V(x)$ exists as in Equation (1) with the parameters $a > 0$, $b > 0$, $0 < \lambda_1 < 1$, and $\lambda_2 > 1$, than the system is fixed time stable.*

$$\dot{V}(x) \leq -aV^{\lambda_1}(x) - bV^{\lambda_2}(x) + \kappa, t \geq 0 \qquad (1)$$

The errors in the system will converge to zero in a fixed time with $\forall 0 < \delta \leq 1$:

$$T_{\max} \leq \frac{1}{a(1 - \lambda_1)} + \frac{1}{b(\lambda_2 - 1)} \qquad (2)$$

Lemma 2. *There is a state of inequality with respect to the following $\rho_i \in \Re$, $i = 1, ..., k$, and $0 < r < 1$:*

$$\left(\sum_{i=1}^{k} |\rho_i| \right)^r \leq \sum_{i=1}^{k} |\rho_i|^r \leq k^{1-r} \left(\sum_{i=1}^{k} |\rho_i| \right)^r \qquad (3)$$

Lemma 3. *There is a state of inequality with respect to the following μ_1, μ_2 are real variables and $x, y, z > 0$:*

$$|\mu_1|^x |\mu_2|^y \leq \frac{x}{x+y} z |\mu_1|^{x+y} + \frac{y}{x+y} z^{\frac{-x}{y}} |\mu_2|^{x+y} \qquad (4)$$

Lemma 4. *There is a state of inequality with respect to the following $a_1 \geq 0$ and $a_2, c > 0$*

$$a_1{}^c(a_2 - a_1) \leq \frac{1}{1+c}(a_2{}^{1+c} - a_1{}^{1+c}) \qquad (5)$$

Lemma 5. *There is a state of inequality with respect to the following $k_1 > 0$, $k_2 \leq k_1$, and $p > 1$*

$$(k_1 - k_2)^p \geq k_2{}^p - k_1{}^p \qquad (6)$$

A number of definitions of fractional operators can be found in the literature. In the current research, the Caputo technique is used for fractional derivation. The Caputo fractional derivative of the αth order of the function $f(t)$ can be expressed as follows [25]:

$$D^\alpha f(t) = \frac{1}{\Gamma(n - \alpha)} \int_0^t \frac{f(\tau)}{(t - \tau)^{\alpha - n + 1}} d\tau \qquad (7)$$

where $\Gamma(\bullet)$ is gamma function and $n - 1 < \alpha < n \in Z^+$. This operator accounts for the memory effects in systems, such as how past states influence present behavior.
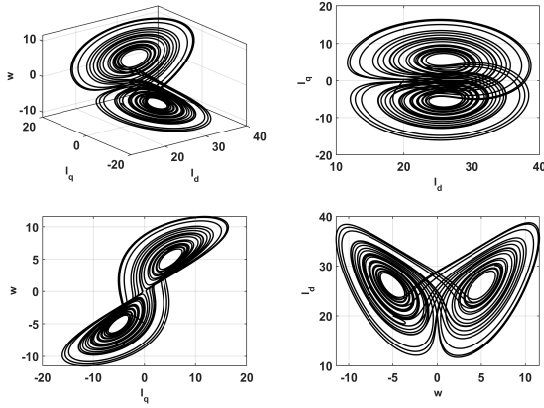
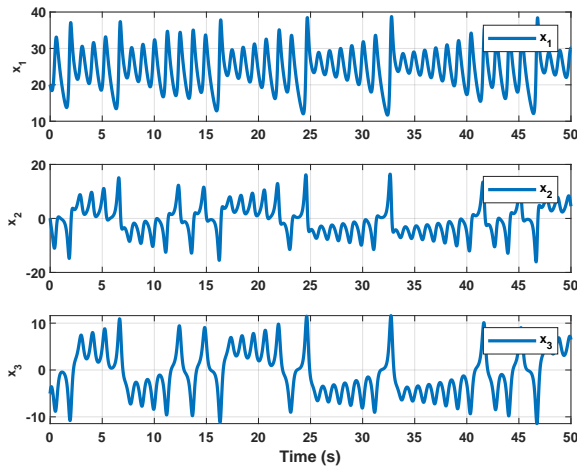Fig. 1. Chaotic behavior of fractional PMSM.

Fig. 2. System states of chaotic fractional PMSM without controllers.

B. Problem formulation

PMSM is an electromechanical system, and its behavior can be represented by the following dynamic model in the $d-q$ reference frame [25] as follows:

$$\frac{di_d}{dt} = -i_d + \omega i_q + u_d$$
$$\frac{di_q}{dt} = -i_q - \omega i_d + \gamma \omega + u_q \quad (8)$$
$$\frac{d\omega}{dt} = \sigma (i_q - \omega) - T_L$$

Here, i_d and i_q are stator currents in the $d-q$ reference frame, ω is the angular velocity of rotor, u_d and u_q are stator voltages in the $d-q$ reference frame, γ and σ are system parameters, T_L is load torque.

To enhance the flexibility of the model design by introducing additional degrees of freedom and providing a more comprehensive understanding of the motor's physical behavior, the above model can be reformulated using fractional-order differentiation as follows:

$$\frac{d^\alpha i_d}{dt^\alpha} = -i_d + \omega i_q + u_d$$
$$\frac{d^\alpha i_q}{dt^\alpha} = -i_q - \omega i_d + \gamma \omega + u_q \quad (9)$$
$$\frac{d^\alpha \omega}{dt^\alpha} = \sigma (i_q - \omega) - T_L$$

Here, α denotes the fractional order. The system presented in Equation (9) exhibits chaotic behavior for the parameter values $\sigma = 5.67$ and $\gamma = 27.1$, with the initial conditions set to $(20, 0.01, -5)$ and fractional order $\alpha = 0.99$ [14]. When $u_d = u_q = T_L = 0$ are assumed along with these parameter values, the system's chaotic behavior is illustrated in Figure 1. Additionally, the changes in system states over time are given in Figure 2.

This study aims to design a fractional-order adaptive fixed-time sliding mode controller for the u_d and u_q control inputs to achieve chaotic synchronization between master-slave fractional-order chaotic PMSM systems, based on the model in Equation (9). Additionally, the proposed controller ensures that the states of the fractional-order PMSM system converge to any specified desired values.

III. Controller Design

This section presents the design of a fractional-order adaptive fixed-time sliding mode controller for synchronization of fractional-order master-slave chaotic PMSM systems. System in Equation (9) can be reformulated for master system with $x_1 = i_d$, $x_2 = i_q$, and $x_3 = \omega$ as follows:

$$\frac{d^\alpha x_1}{dt^\alpha} = -x_1 + x_3 x_2$$
$$\frac{d^\alpha x_2}{dt^\alpha} = -x_2 - x_3 x_1 + \gamma x_3 \quad (10)$$
$$\frac{d^\alpha x_3}{dt^\alpha} = \sigma (x_2 - x_3)$$

Note that for the master system control inputs and load torque are taken as zero. Dynamic equations of slave system can be written with $y_1 = i_d$, $y_2 = i_q$, and $y_3 = \omega$ as follows:

$$\frac{d^\alpha y_1}{dt^\alpha} = -y_1 + y_3 y_2 + u_d$$
$$\frac{d^\alpha y_2}{dt^\alpha} = -y_2 - y_3 y_1 + \gamma y_3 + u_q \quad (11)$$
$$\frac{d^\alpha y_3}{dt^\alpha} = \sigma (y_2 - y_3) - T_L$$

Let the synchronization errors be $e_1 = y_1 - x_1$, $e_2 = y_2 - x_2$, and $e_3 = y_3 - x_3$.

The design of the sliding surface functions, which form the foundation of the proposed controller structure, is presented as follows:

$$s_1 = D^{\alpha-1} e_1$$
$$+ D^{\alpha-2} \left(\beta_{11} |e_1|^{\sigma_1} sign(e_1) + \beta_{12} |e_1|^{\sigma_2} sign(e_1) \right)$$
$$s_2 = D^{\alpha-1} e_2$$
$$+ D^{\alpha-2} \left(\beta_{21} |e_2|^{\sigma_1} sign(e_2) + \beta_{22} |e_2|^{\sigma_2} sign(e_2) \right)$$
$$(12)$$

where $\beta_{i1}, \beta_{i2}, \sigma_1$, and σ_2 are positive constants with ($i = 1, 2$), and $\sigma_1 \in (0, 1)$, $\sigma_2 \in (1, 2)$.

Remark 1. *Since the control inputs u_d and u_q appear in the first two expressions of Equation (11), it will be sufficient to define two sliding surface functions to obtain these inputs in the controller design.*

Theorem 1. *Consider the sliding surface functions in Equation (12), according to Lemma (1), the error dynamics will converge to zero within a fixed time.*

Proof. When the error dynamics are on sliding surfaces ($s_i = 0$), the following equality holds:

$$D^{\alpha-1}e_i = -D^{\alpha-2}\left(\beta_{i1}|e_i|^{\sigma_1}sign(e_i) + \beta_{i2}|e_i|^{\sigma_2}sign(e_i)\right) \tag{13}$$

Evaluate the Lyapunov function for errors as follows:

$$V_i = |e_i| \tag{14}$$

The Lyapunov function's derivative may be calculated as:

$$
\begin{aligned}
\dot{V}_i &= \dot{e}_i sign(e_i) \\
&= \left(D^{2-\alpha}\left(D^{\alpha-1}e_i\right)\right)sign(e_i) \\
&= \left(D^{2-\alpha}\left(-D^{2-\alpha}\left(\beta_{i1}|e_i|^{\sigma_1}sign(e_i) + \beta_{i2}|e_i|^{\sigma_2}sign(e_i)\right)\right)\right)sign(e_i)
\end{aligned} \tag{15}
$$

Here, using $e_i sign(e_i) = |e_i|$, and $sign(e_i)sign(e_i) = 1$, Equation (15) can be rearranged as:

$$\dot{V}_i = -\beta_{i1}|e_i|^{\sigma_1} - \beta_{i2}|e_i|^{\sigma_2} \tag{16}$$

Hence, based on Lemma (1), the fixed-time convergence is proven, and the proof is completed. $\square$

For sliding surface functions specified in Equation (12), reaching laws are chosen as follows:

$$\dot{s}_i = -k_{i1}|s_i|^p sign(s_i) - k_{i2}|s_i|^q sign(s_i) \tag{17}$$

where k_{i1}, k_{i2}, p, and q. are positive constants with $i = 1, 2$ and $p \in (0, 1)$, $q \in (1, 2)$.

In order to carry out the controller design, the error dynamics must be defined. Using Equation (10) and Equation (11), the error dynamics of the master-slave PMSM system can be obtained as follows:

$$
\begin{aligned}
\frac{d^{\alpha}e_1}{dt^{\alpha}} &= -a_1 e_1 + c_1(y_3 y_2 - x_3 x_2) + u_d \\
\frac{d^{\alpha}e_2}{dt^{\alpha}} &= -a_2 e_2 - c_2(y_3 y_1 - x_3 x_1) + \gamma e_3 + u_q \\
\frac{d^{\alpha}e_3}{dt^{\alpha}} &= \sigma e_2 - \sigma e_3 - T_L
\end{aligned} \tag{18}
$$

a_1, c_1, a_2, c_2, and γ are system parameters and positive constants. These parameters will be considered as unknown values in the controller design and will be estimated by adaptive laws. Considering the sliding surfaces in Equation (12), the reaching laws in Equation (17), and the error dynamics in Equation (18), the fractional order adaptive fixed time sliding mode control inputs can be designed as follows:

$$
\begin{aligned}
u_d &= \hat{a}_1 e_1 - \hat{c}_1(y_3 y_2 - x_3 x_2) \\
&\quad - D^{\alpha-1}\left(\beta_{11}sign(e_1)|e_1|^p + \beta_{12}sign(e_1)|e_1|^q\right) \\
&\quad - k_{11}sign(s_1)|s_1|^p - k_{12}sign(s_1)|s_1|^q \\
u_q &= \hat{a}_2 e_2 + \hat{c}_2(y_1 y_3 - x_1 x_3) - \hat{\gamma}e_3 \\
&\quad - D^{\alpha-1}\left(\beta_{21}sign(e_2)|e_2|^p + \beta_{22}sign(e_2)|e_2|^q\right) \\
&\quad - k_{21}sign(s_2)|s_2|^p - k_{22}sign(s_2)|s_2|^q
\end{aligned} \tag{19}
$$

Furthermore, the parametric adaptation rules are provided as:

$$
\begin{aligned}
\dot{\hat{a}}_1 &= -\lambda_{11}\hat{a}_1^p - \lambda_{12}\hat{a}_1^q + \lambda_{13}s_1 e_1 \\
\dot{\hat{c}}_1 &= -\eta_{11}\hat{c}_1^p - \eta_{12}\hat{c}_1^q - \eta_{13}(y_2 y_3 - x_2 x_3)s_1 \\
\dot{\hat{a}}_2 &= -\lambda_{21}\hat{a}_2^p - \lambda_{22}\hat{a}_2^q + \lambda_{23}s_2 e_2 \\
\dot{\hat{c}}_2 &= -\eta_{21}\hat{c}_2^p - \eta_{22}\hat{c}_2^q + \eta_{23}(y_1 y_3 - x_1 x_3)s_2 \\
\dot{\hat{\gamma}} &= -\mu_{11}\hat{\gamma}^p - \mu_{12}\hat{\gamma}^q - \mu_{13}s_2 e_3
\end{aligned} \tag{20}
$$

Here, $\lambda_{11}, \lambda_{12}, \lambda_{13}, \eta_{11}, \eta_{12}, \eta_{13}, \lambda_{21}, \lambda_{22}, \lambda_{23}, \eta_{21}, \eta_{22}, \eta_{23}, \mu_{11}, \mu_{12}, \mu_{13} > 0$.

Theorem 2. *Consider the master-slave PMSMs in Equation (10) and Equation (11). If we use the controllers Equation (19) in conjunction with the parametric adaptation laws in Equation (20), the resultant closed-loop system is fixed-time stable, and all sliding surface variables in the closed-loop system may regulate to tiny residual sets around zero in fixed time.*

Proof. Consider the Lyapunov function as follows:

$$
\begin{aligned}
V &= \frac{1}{2}s_1^2 + \frac{1}{2}s_2^2 + \frac{1}{2\lambda_{13}}\tilde{a}_1^2 \\
&\quad + \frac{1}{2\lambda_{23}}\tilde{a}_2^2 + \frac{1}{2\eta_{13}}\tilde{c}_1^2 + \frac{1}{2\eta_{23}}\tilde{c}_2^2 + \frac{1}{2\mu_{13}}\tilde{\gamma}^2
\end{aligned} \tag{21}
$$

Here, $\tilde{a}_1 = a_1 - \hat{a}_1, \tilde{a}_2 = a_2 - \hat{a}_2, \tilde{c}_1 = c_1 - \hat{c}_1, \tilde{c}_2 = c_2 - \hat{c}_2, \tilde{\gamma} = \gamma - \hat{\gamma}$ parameter estimation errors of parameters $a_1, a_2, c_1, c_2, \gamma$, respectively. Since these parameters are constants, time derivations of estimation errors will be $\dot{\tilde{a}}_1 = -\dot{\hat{a}}_1, \dot{\tilde{a}}_2 = -\dot{\hat{a}}_2, \dot{\tilde{c}}_1 = -\dot{\hat{c}}_1, \dot{\tilde{c}}_2 = -\dot{\hat{c}}_2, \dot{\tilde{\gamma}} = -\dot{\hat{\gamma}}$, respectively.

Hence, the time derivative of Equation (21) can be written as follows, taking into account the derivations of estimation errors:

$$
\begin{aligned}
\dot{V} &= s_1\dot{s}_1 + s_2\dot{s}_2 - \frac{1}{\lambda_{13}}\tilde{a}_1\dot{\hat{a}}_1 \\
&\quad - \frac{1}{\lambda_{23}}\tilde{a}_2\dot{\hat{a}}_2 - \frac{1}{\eta_{13}}\tilde{c}_1\dot{\hat{c}}_1 - \frac{1}{\eta_{23}}\tilde{c}_2\dot{\hat{c}}_2 - \frac{1}{\mu_{13}}\tilde{\gamma}\dot{\hat{\gamma}}
\end{aligned} \tag{22}
$$

Using the derivatives of sliding surface functions defined in Equation (12) and the error dynamics defined in Equation (18), Equation (22) can be written as follows:

$$\dot{V} = s_1 \begin{pmatrix} -a_1 e_1 + c_1 (y_3 y_2 - x_3 x_2) + u_d \\ + D^{\alpha-1} (\beta_{11} |e_1|^{\sigma_1} sign(e_1) + \beta_{12} |e_1|^{\sigma_2} sign(e_1)) \end{pmatrix}$$
$$+ s_2 \begin{pmatrix} -a_2 e_2 - c_2 (y_3 y_1 - x_3 x_1) + \gamma e_3 + u_q \\ + D^{\alpha-1} (\beta_{21} |e_2|^{\sigma_1} sign(e_2) + \beta_{22} |e_2|^{\sigma_2} sign(e_2)) \end{pmatrix}$$
$$- \frac{1}{\lambda_{13}} \tilde{a}_1 \dot{\hat{a}}_1 - \frac{1}{\lambda_{23}} \tilde{a}_2 \dot{\hat{a}}_2 - \frac{1}{\eta_{13}} \tilde{c}_1 \dot{\hat{c}}_1 - \frac{1}{\eta_{23}} \tilde{c}_2 \dot{\hat{c}}_2 - \frac{1}{\mu_{13}} \tilde{\gamma} \dot{\hat{\gamma}} \tag{23}$$

Furthermore, using the controller inputs in Equation (19), Equation (23) can be written as follows:

$$\dot{V} = s_1 \begin{pmatrix} -a_1 e_1 + c_1 (y_3 y_2 - x_3 x_2) + \hat{a}_1 e_1 - \hat{c}_1 (y_3 y_2 - x_3 x_2) \\ - D^{\alpha-1} (\beta_{11} sign(e_1) |e_1|^p + \beta_{12} sign(e_1) |e_1|^q) \\ - k_{11} sign(s_1) |s_1|^p - k_{12} sign(s_1) |s_1|^q \\ + D^{\alpha-1} (\beta_{11} |e_1|^{\sigma_1} sign(e_1) + \beta_{12} |e_1|^{\sigma_2} sign(e_1)) \end{pmatrix}$$
$$+ s_2 \begin{pmatrix} -a_2 e_2 - c_2 (y_3 y_1 - x_3 x_1) + \gamma e_3 + \hat{a}_2 e_2 + \hat{c}_2 (y_1 y_3 - x_1 x_3) \\ - \hat{\gamma} e_3 - D^{\alpha-1} (\beta_{11} sign(e_2) |e_2|^p + \beta_{12} sign(e_2) |e_2|^q) \\ - k_{21} sign(s_2) |s_2|^p - k_{22} sign(s_2) |s_2|^q \\ + D^{\alpha-1} (\beta_{21} |e_2|^{\sigma_1} sign(e_2) + \beta_{22} |e_2|^{\sigma_2} sign(e_2)) \end{pmatrix}$$
$$- \frac{1}{\lambda_{13}} \tilde{a}_1 \dot{\hat{a}}_1 - \frac{1}{\lambda_{23}} \tilde{a}_2 \dot{\hat{a}}_2 - \frac{1}{\eta_{13}} \tilde{c}_1 \dot{\hat{c}}_1 - \frac{1}{\eta_{23}} \tilde{c}_2 \dot{\hat{c}}_2 - \frac{1}{\mu_{13}} \tilde{\gamma} \dot{\hat{\gamma}} \tag{24}$$

Here, it is assumed that $\sigma_1 = p$ and $\sigma_2 = q$. Also using $s_i sign(s_i) = |s_i|$, Equation (24) can be simplified as follows:

$$\dot{V} = \begin{pmatrix} -a_1 e_1 s_1 + c_1 (y_3 y_2 - x_3 x_2) s_1 \\ + \hat{a}_1 e_1 s_1 - \hat{c}_1 (y_3 y_2 - x_3 x_2) s_1 \\ - k_{11} |s_1|^{p+1} - k_{12} |s_1|^{q+1} \end{pmatrix}$$
$$+ \begin{pmatrix} -a_2 e_2 s_2 - c_2 (y_3 y_1 - x_3 x_1) s_2 \\ + \gamma e_3 s_2 + \hat{a}_2 e_2 s_2 + \hat{c}_2 (y_1 y_3 - x_1 x_3) s_2 \\ - \hat{\gamma} e_3 s_2 - k_{21} |s_2|^{p+1} - k_{22} |s_2|^{q+1} \end{pmatrix}$$
$$- \frac{1}{\lambda_{13}} \tilde{a}_1 \dot{\hat{a}}_1 - \frac{1}{\lambda_{23}} \tilde{a}_2 \dot{\hat{a}}_2 - \frac{1}{\eta_{13}} \tilde{c}_1 \dot{\hat{c}}_1 - \frac{1}{\eta_{23}} \tilde{c}_2 \dot{\hat{c}}_2 - \frac{1}{\mu_{13}} \tilde{\gamma} \dot{\hat{\gamma}} \tag{25}$$

Here, using the adaptive rules in Equation (20), Equation (25) can be rearranged as follows:

$$\dot{V} = -k_{11} |s_1|^{p+1} - k_{12} |s_1|^{q+1} - k_{21} |s_2|^{p+1} - k_{22} |s_2|^{q+1}$$
$$+ \frac{\lambda_{11}}{\lambda_{13}} \tilde{a}_1 \hat{a}_1^p + \frac{\lambda_{12}}{\lambda_{13}} \tilde{a}_1 \hat{a}_1^q + \frac{\eta_{11}}{\eta_{13}} \tilde{c}_1 \hat{c}_1^p + \frac{\eta_{12}}{\eta_{13}} \tilde{c}_1 \hat{c}_1^q$$
$$+ \frac{\lambda_{21}}{\lambda_{23}} \tilde{a}_2 \hat{a}_2^p + \frac{\lambda_{22}}{\lambda_{23}} \tilde{a}_2 \hat{a}_2^q + \frac{\eta_{21}}{\eta_{23}} \tilde{c}_2 \hat{c}_2^p + \frac{\eta_{22}}{\eta_{23}} \tilde{c}_2 \hat{c}_2^q$$
$$+ \frac{\mu_{11}}{\mu_{13}} \tilde{\gamma} \hat{\gamma}^p + \frac{\mu_{12}}{\mu_{13}} \tilde{\gamma} \hat{\gamma}^q \tag{26}$$

Furthermore, considering Lemmas 4 and 5, the following inequalities exist:

$$\tilde{a}_1 \hat{a}_1^p \le \frac{1}{1+p} \left(2a_1^{p+1} - \tilde{a}_1^{p+1} \right), \tilde{c}_1 \hat{c}_1^p \le \frac{1}{1+p} \left(2c_1^{p+1} - \tilde{c}_1^{p+1} \right)$$
$$\tilde{a}_1 \hat{a}_1^q \le \frac{1}{1+q} \left(2a_1^{q+1} - \tilde{a}_1^{q+1} \right), \tilde{c}_1 \hat{c}_1^q \le \frac{1}{1+q} \left(2c_1^{q+1} - \tilde{c}_1^{q+1} \right)$$
$$\tilde{a}_2 \hat{a}_2^p \le \frac{1}{1+p} \left(2a_2^{p+1} - \tilde{a}_2^{p+1} \right), \tilde{c}_2 \hat{c}_2^p \le \frac{1}{1+p} \left(2c_2^{p+1} - \tilde{c}_2^{p+1} \right)$$
$$\tilde{a}_2 \hat{a}_2^q \le \frac{1}{1+q} \left(2a_2^{q+1} - \tilde{a}_2^{q+1} \right), \tilde{c}_2 \hat{c}_2^q \le \frac{1}{1+q} \left(2c_2^{q+1} - \tilde{c}_2^{q+1} \right)$$
$$\tilde{\gamma} \hat{\gamma}^p \le \frac{1}{1+p} \left(2\gamma^{p+1} - \tilde{\gamma}^{p+1} \right), \ \tilde{\gamma} \hat{\gamma}^q \le \frac{1}{1+q} \left(2\gamma^{q+1} - \tilde{\gamma}^{q+1} \right) \tag{27}$$

Equation (26) may be reformulated using the inequalities stated in Equation (27) as follows:

$$\dot{V} \le -k_{11} |s_1|^{p+1} - k_{12} |s_1|^{q+1} - k_{21} |s_2|^{p+1} - k_{22} |s_2|^{q+1}$$
$$+ \frac{\lambda_{11}}{\lambda_{13}(1+p)} \left(2a_1^{p+1} - \tilde{a}_1^{p+1} \right) + \frac{\lambda_{12}}{\lambda_{13}(1+q)} \left(2a_1^{q+1} - \tilde{a}_1^{q+1} \right)$$
$$+ \frac{\eta_{11}}{\eta_{13}(1+p)} \left(2c_1^{p+1} - \tilde{c}_1^{p+1} \right) + \frac{\eta_{12}}{\eta_{13}(1+q)} \left(2c_1^{q+1} - \tilde{c}_1^{q+1} \right)$$
$$+ \frac{\lambda_{21}}{\lambda_{23}(1+p)} \left(2a_2^{p+1} - \tilde{a}_2^{p+1} \right) + \frac{\lambda_{22}}{\lambda_{23}(1+q)} \left(2a_2^{q+1} - \tilde{a}_2^{q+1} \right)$$
$$+ \frac{\eta_{21}}{\eta_{23}(1+p)} \left(2c_2^{p+1} - \tilde{c}_2^{p+1} \right) + \frac{\eta_{22}}{\eta_{23}(1+q)} \left(2c_2^{q+1} - \tilde{c}_2^{q+1} \right)$$
$$+ \frac{\mu_{11}}{\mu_{13}(1+p)} \left(2\gamma^{p+1} - \tilde{\gamma}^{p+1} \right) + \frac{\mu_{12}}{\mu_{13}(1+q)} \left(2\gamma^{q+1} - \tilde{\gamma}^{q+1} \right) \tag{28}$$

Rearrange Equation (28) as follows:

$$\dot{V} \le -k_{11} |s_1|^{p+1} - k_{12} |s_1|^{q+1} - k_{21} |s_2|^{p+1} - k_{22} |s_2|^{q+1}$$
$$+ \frac{\lambda_{11} 2a_1^{p+1}}{\lambda_{13}(1+p)} - \frac{\lambda_{11}}{\lambda_{13}(1+p)} \tilde{a}_1^{p+1} + \frac{\lambda_{12} 2a_1^{q+1}}{\lambda_{13}(1+q)} - \frac{\lambda_{12}}{\lambda_{13}(1+q)} \tilde{a}_1^{q+1}$$
$$+ \frac{\eta_{11} 2c_1^{p+1}}{\eta_{13}(1+p)} - \frac{\eta_{11}}{\eta_{13}(1+p)} \tilde{c}_1^{p+1} + \frac{\eta_{12} 2c_1^{q+1}}{\eta_{13}(1+q)} - \frac{\eta_{12}}{\eta_{13}(1+q)} \tilde{c}_1^{q+1}$$
$$+ \frac{\lambda_{21} 2a_2^{p+1}}{\lambda_{23}(1+p)} - \frac{\lambda_{21}}{\lambda_{23}(1+p)} \tilde{a}_2^{p+1} + \frac{\lambda_{22} 2a_2^{q+1}}{\lambda_{23}(1+q)} - \frac{\lambda_{22}}{\lambda_{23}(1+q)} \tilde{a}_2^{q+1}$$
$$+ \frac{\eta_{21} 2c_2^{p+1}}{\eta_{23}(1+p)} - \frac{\eta_{21}}{\eta_{23}(1+p)} \tilde{c}_2^{p+1} + \frac{\eta_{22} 2c_2^{q+1}}{\eta_{23}(1+q)} - \frac{\eta_{22}}{\eta_{23}(1+q)} \tilde{c}_2^{q+1}$$
$$+ \frac{\mu_{11} 2\gamma^{p+1}}{\mu_{13}(1+p)} - \frac{\mu_{11}}{\mu_{13}(1+p)} \tilde{\gamma}^{p+1} + \frac{\mu_{12} 2\gamma^{q+1}}{\mu_{13}(1+q)} - \frac{\mu_{12}}{\mu_{13}(1+q)} \tilde{\gamma}^{q+1} \tag{29}$$

Furthermore, considering Lemmas 2 and 3 , the following inequalities exist:

$$\tilde{a}_1^{p+1} \le 2^{\frac{p+1}{2}} \left(\frac{1}{2} \tilde{a}_1^2 \right)^{\frac{p+1}{2}}, \tilde{c}_1^{p+1} \le 2^{\frac{p+1}{2}} \left(\frac{1}{2} \tilde{c}_1^2 \right)^{\frac{p+1}{2}}$$

$$\tilde{a}_1^{q+1} \le 2^{\frac{q+1}{2}} \left(\frac{1}{2} \tilde{a}_1^2 \right)^{\frac{q+1}{2}}, \tilde{c}_1^{q+1} \le 2^{\frac{q+1}{2}} \left(\frac{1}{2} \tilde{c}_1^2 \right)^{\frac{q+1}{2}}$$

$$\tilde{a}_2^{p+1} \le 2^{\frac{p+1}{2}} \left(\frac{1}{2} \tilde{a}_2^2 \right)^{\frac{p+1}{2}}, \tilde{c}_2^{p+1} \le 2^{\frac{p+1}{2}} \left(\frac{1}{2} \tilde{c}_2^2 \right)^{\frac{p+1}{2}}$$

$$\tilde{a}_2^{q+1} \le 2^{\frac{q+1}{2}} \left(\frac{1}{2} \tilde{a}_2^2 \right)^{\frac{q+1}{2}}, \tilde{c}_2^{q+1} \le 2^{\frac{q+1}{2}} \left(\frac{1}{2} \tilde{c}_2^2 \right)^{\frac{q+1}{2}}$$

$$\tilde{\gamma}^{p+1} \leq 2^{\frac{p+1}{2}} \left(\frac{1}{2}\tilde{\gamma}^2\right)^{\frac{p+1}{2}}, \quad \tilde{\gamma}^{q+1} \leq 2^{\frac{q+1}{2}} \left(\frac{1}{2}\tilde{\gamma}^2\right)^{\frac{q+1}{2}}$$

$$|s_1|^{p+1} \leq 2^{\frac{p+1}{2}} \left(\frac{1}{2}s_1^2\right)^{\frac{p+1}{2}}, |s_1|^{q+1} \leq 2^{\frac{q+1}{2}} \left(\frac{1}{2}s_1^2\right)^{\frac{q+1}{2}}$$

$$|s_2|^{p+1} \leq 2^{\frac{p+1}{2}} \left(\frac{1}{2}s_2^2\right)^{\frac{p+1}{2}}, |s_2|^{q+1} \leq 2^{\frac{q+1}{2}} \left(\frac{1}{2}s_2^2\right)^{\frac{q+1}{2}} \tag{30}$$

Equation (29) may be reformulated using the inequalities stated in Equation (30) as follows:

$$\dot{V} \leq -k_{11}2^{\frac{p+1}{2}}\left(\frac{1}{2}s_1^2\right)^{\frac{p+1}{2}} - k_{12}2^{\frac{q+1}{2}}\left(\frac{1}{2}s_1^2\right)^{\frac{q+1}{2}}$$

$$- k_{21}2^{\frac{p+1}{2}}\left(\frac{1}{2}s_2^2\right)^{\frac{p+1}{2}} - k_{22}2^{\frac{q+1}{2}}\left(\frac{1}{2}s_2^2\right)^{\frac{q+1}{2}}$$

$$- \frac{\lambda_{11}2^{\frac{p+1}{2}}}{\lambda_{13}(1+p)}\left(\frac{1}{2}\tilde{a}_1^2\right)^{\frac{p+1}{2}} - \frac{\lambda_{12}2^{\frac{q+1}{2}}}{\lambda_{13}(1+q)}\left(\frac{1}{2}\tilde{a}_1^2\right)^{\frac{q+1}{2}}$$

$$- \frac{\eta_{11}2^{\frac{p+1}{2}}}{\eta_{13}(1+p)}\left(\frac{1}{2}\tilde{c}_1^2\right)^{\frac{p+1}{2}} - \frac{\eta_{12}2^{\frac{q+1}{2}}}{\eta_{13}(1+q)}\left(\frac{1}{2}\tilde{c}_1^2\right)^{\frac{q+1}{2}}$$

$$- \frac{\lambda_{21}2^{\frac{p+1}{2}}}{\lambda_{23}(1+p)}\left(\frac{1}{2}\tilde{a}_2^2\right)^{\frac{p+1}{2}} - \frac{\lambda_{22}2^{\frac{q+1}{2}}}{\lambda_{23}(1+q)}\left(\frac{1}{2}\tilde{a}_2^2\right)^{\frac{q+1}{2}} \tag{31}$$

$$- \frac{\eta_{21}2^{\frac{p+1}{2}}}{\eta_{23}(1+p)}\left(\frac{1}{2}\tilde{c}_2^2\right)^{\frac{p+1}{2}} - \frac{\eta_{22}2^{\frac{q+1}{2}}}{\eta_{23}(1+q)}\left(\frac{1}{2}\tilde{c}_2^2\right)^{\frac{q+1}{2}}$$

$$- \frac{\mu_{11}2^{\frac{p+1}{2}}}{\mu_{13}(1+p)}\left(\frac{1}{2}\tilde{\gamma}^2\right)^{\frac{p+1}{2}} - \frac{\mu_{12}2^{\frac{q+1}{2}}}{\mu_{13}(1+q)}\left(\frac{1}{2}\tilde{\gamma}^2\right)^{\frac{q+1}{2}}$$

$$+ \frac{\lambda_{11}2a_1^{p+1}}{\lambda_{13}(1+p)} + \frac{\lambda_{12}2a_1^{q+1}}{\lambda_{13}(1+q)} + \frac{\eta_{11}2c_1^{p+1}}{\eta_{13}(1+p)} + \frac{\eta_{12}2c_1^{q+1}}{\eta_{13}(1+q)}$$

$$+ \frac{\lambda_{21}2a_2^{p+1}}{\lambda_{23}(1+p)} + \frac{\lambda_{22}2a_2^{q+1}}{\lambda_{23}(1+q)} + \frac{\eta_{21}2c_2^{p+1}}{\eta_{23}(1+p)} + \frac{\eta_{22}2c_2^{q+1}}{\eta_{23}(1+q)}$$

$$+ \frac{\mu_{11}2\gamma^{p+1}}{\mu_{13}(1+p)} + \frac{\mu_{12}2\gamma^{q+1}}{\mu_{13}(1+q)}$$

Therefore, Equation (31) can be written in following form:

$$\dot{V}(x) \leq -\bar{a}V^{\bar{\lambda}_1}(x) - \bar{b}V^{\bar{\lambda}_2}(x) + \bar{\kappa} \tag{32}$$

Here,

$$-\bar{a} = \min\left\{ \begin{array}{c} -k_{11}2^{\frac{p+1}{2}}, -k_{21}2^{\frac{p+1}{2}}, -\frac{\lambda_{11}2^{\frac{p+1}{2}}}{\lambda_{13}(1+p)}, -\frac{\eta_{11}2^{\frac{p+1}{2}}}{\eta_{13}(1+p)}, \\ -\frac{\lambda_{21}2^{\frac{p+1}{2}}}{\lambda_{23}(1+p)}, -\frac{\eta_{21}2^{\frac{p+1}{2}}}{\eta_{23}(1+p)}, -\frac{\mu_{11}2^{\frac{p+1}{2}}}{\mu_{13}(1+p)} \end{array} \right\},$$

$$-\bar{b} = \min\left\{ \begin{array}{c} -k_{12}2^{\frac{q+1}{2}}, -k_{22}2^{\frac{q+1}{2}}, -\frac{\lambda_{12}2^{\frac{q+1}{2}}}{\lambda_{13}(1+q)}, -\frac{\eta_{12}2^{\frac{q+1}{2}}}{\eta_{13}(1+q)}, \\ -\frac{\lambda_{22}2^{\frac{q+1}{2}}}{\lambda_{23}(1+q)}, -\frac{\eta_{22}2^{\frac{q+1}{2}}}{\eta_{23}(1+q)}, -\frac{\mu_{12}2^{\frac{q+1}{2}}}{\mu_{13}(1+q)} \end{array} \right\},$$

$$\bar{\kappa} = + \frac{\lambda_{11}2a_1^{p+1}}{\lambda_{13}(1+p)} + \frac{\lambda_{12}2a_1^{q+1}}{\lambda_{13}(1+q)} + \frac{\eta_{11}2c_1^{p+1}}{\eta_{13}(1+p)} + \frac{\eta_{12}2c_1^{q+1}}{\eta_{13}(1+q)}$$

$$+ \frac{\lambda_{21}2a_2^{p+1}}{\lambda_{23}(1+p)} + \frac{\lambda_{22}2a_2^{q+1}}{\lambda_{23}(1+q)} + \frac{\eta_{21}2c_2^{p+1}}{\eta_{23}(1+p)} + \frac{\eta_{22}2c_2^{q+1}}{\eta_{23}(1+q)}$$

$$+ \frac{\mu_{11}2\gamma^{p+1}}{\mu_{13}(1+p)} + \frac{\mu_{12}2\gamma^{q+1}}{\mu_{13}(1+q)},$$

$$\bar{\lambda}_1 = \frac{p+1}{2}, \bar{\lambda}_2 = \frac{q+1}{2}$$

Thus, according to lemma 1, all sliding surface functions and estimation errors will converge to a close neighborhood of zero in fixed time. This concludes the proof.

□

IV. SIMULATIONS

To evaluate the performance of the proposed controllers, simulations were conducted on a fractional-order chaotic Permanent Magnet Synchronous Motor (PMSM). The results are presented for various scenarios. All simulations were implemented within the MATLAB/SIMULINK environment. Furthermore, the Fractional Order Transfer Function (FOTF) Toolbox developed in [26] was used to perform fractional derivative and integral operations. Initial conditions for master-slave PMSM are chosen as: $x_1(0) = 20, x_2(0) = 0.01, x_3(0) = -5, y_1(0) = 25, y_2(0) = 0.2, y_3(0) = -1$. Controller parameters in Equation (19) are selected as: $\beta_{11} = \beta_{12} = \beta_{21} = \beta_{22} = 5, k_{11} = k_{12} = k_{21} = k_{22} = 5, \sigma_1 = p = 0.5, \sigma_2 = q = 1.5$. The fractional order was chosen to be $\alpha = 0.99$ in every simulation. The gains of adaptive laws are taken as: $\lambda_{11} = \lambda_{12} = \lambda_{13} = \eta_{11} = \eta_{12} = \eta_{13} = \lambda_{21} = \lambda_{22} = \lambda_{23} = \eta_{21} = \eta_{22} = \eta_{23} = \mu_{11} = \mu_{12} = \mu_{13} = 0.01$ and initial values for adaptive parameters are set to: $\hat{a}_1(0) = 0, \hat{c}_1(0) = 0, \hat{a}_2(0) = 0, \hat{c}_2(0) = 0, \hat{\gamma}(0) = 0$. Simulation studies were carried out as follows, considering different situations.

Case 1: Chaotic synchronization

In the first scenario, the synchronization of fractional-order chaotic master-slave PMSM systems is analyzed, as described by Equations (10) and (11). This type of synchronization is particularly useful in applications such as multi-motor systems in robotics, where synchronized operation is essential for precision tasks. Synchronized joint operation, for example, is critical in robotic arms for smooth motion and accurate job execution, while synchronized motors ensure constant operation, preventing misalignment or mechanical damage in conveyor belts or packing systems.

In this case, the load torque T_L is set to zero, with the objective of evaluating the synchronization achieved when the control signals, formulated in Equation (19), are applied to the systems. The simulation time for Case 1 is selected as 10 seconds.

Figure 3 illustrates the evolution of the system states for both PMSMs over time. The application of the proposed controller demonstrates its effectiveness, as the states of the slave PMSM rapidly synchronize with those of the master
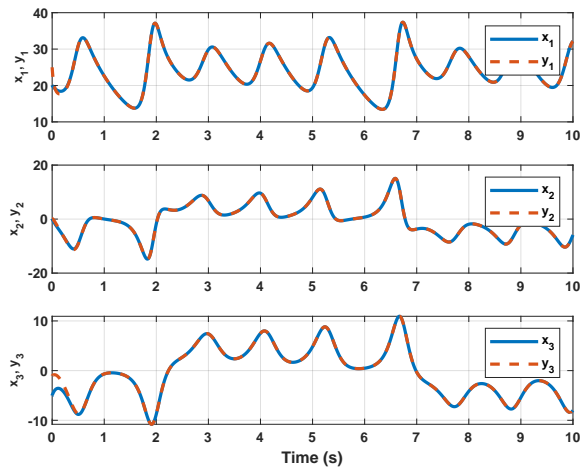
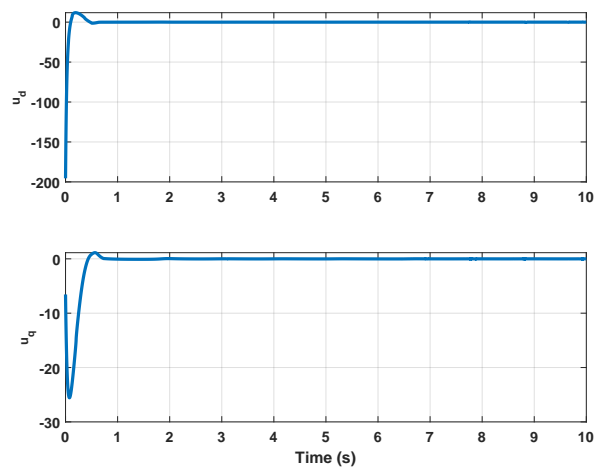Fig. 3. System states for synchronization.

Fig. 5. Control inputs for synchronization.

PMSM. Similarly, Figure 4 presents the synchronization errors between the fractional-order master and slave PMSMs. The results indicate that the errors converge to zero with notable speed and precision.
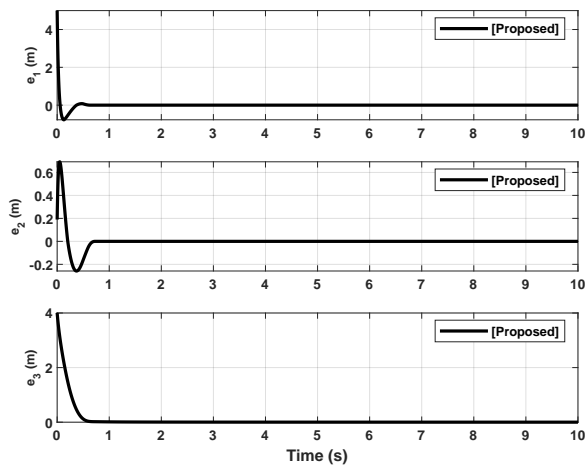

Fig. 4. Synchronization errors.

Fig. 6. Convergences of adaptive parameters.

Figure 5 illustrates the variation of the control inputs associated with the proposed controller.

Figure 6 shows the evolution of the adaptive parameters over time. As is evident in the figure, the adaptive parameters exhibit successful convergence.

Case 2: Controller comparison

In the second scenario, the performance of the proposed controller structure is compared with that of alternative control approaches. In this simulation, the load torque T_L is again set to zero. For this purpose, the proposed controller is compared with a finite-time control approach from the literature [27] and an adaptive fixed-time control approach. The input parameters for the adaptive fixed-time controller are configured as follows:
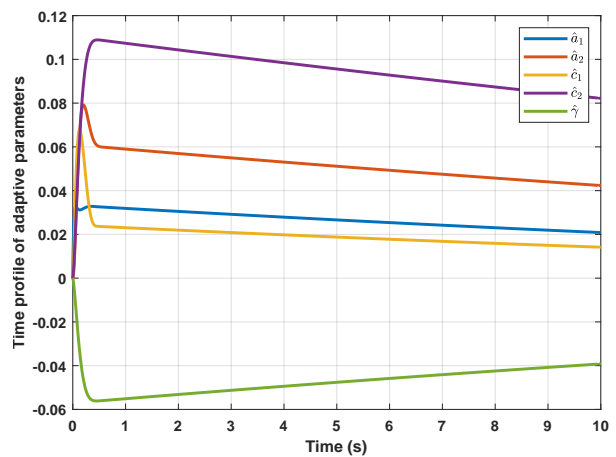
$$u_d = \hat{a}_{11}e_1 - \hat{c}_1(y_2y_3 - x_2x_3)$$
$$\quad - k_{11}\,\text{sign}(e_1)|e_1|^p - k_{12}\,\text{sign}(e_1)|e_1|^q$$
$$u_q = \hat{a}_{21}e_2 + \hat{c}_2(y_1y_3 - x_1x_3) - \hat{\gamma}e_3$$
$$\quad - k_{21}\,\text{sign}(e_2)\,|e_2|^p - k_{22}\,\text{sign}(e_2)|e_2|^q$$

To ensure a fair comparison, the controller parameters are set to the same values as those specified at the beginning of this section for the proposed controller.

Figure 7 illustrates the time variations of the fractional-order chaotic master-slave PMSM system under different control inputs. As observed, the proposed controller achieves significantly better convergence than the finite-time control approach. Moreover, it ensures faster convergence of the error dynamics compared to the integer-order fixed-time control structure.

Figure 8 presents the time variations of control signals for the three control approaches. It is evident that the proposed control structure demonstrates superior performance in terms of responsiveness compared to the other control signals.
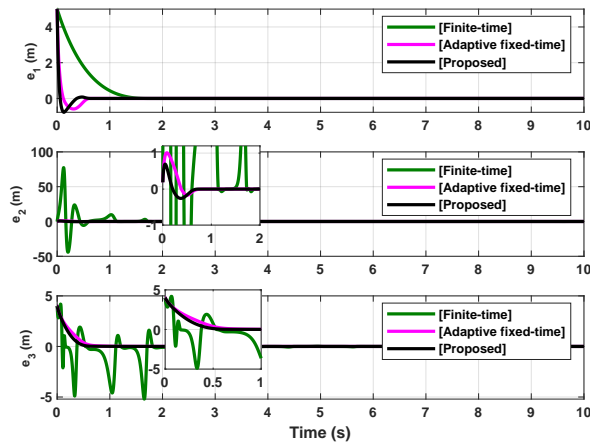
https://dergipark.org.tr/bajece

Fig. 7. Synchronization errors for different controllers.
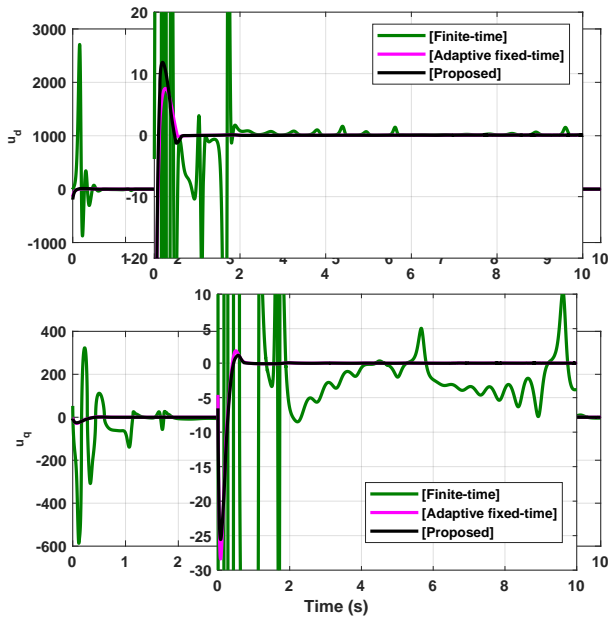

Fig. 8. Control inputs for different controllers.

Case 3: Performance under load torque

In the third scenario, the performance of the fractional-order chaotic PMSM system under different load values was evaluated using the proposed controller. This scenario assesses the controller's ability to maintain synchronization under varying loads, a common challenge in real-world systems. Practical relevance includes, renewable energy systems, such as in wind turbines or hydroelectric generators, load fluctuations occur due to changes in environmental conditions. The proposed controller ensures stable power generation despite such variability. Moreover in heavy machinery systems, equipment operating under dynamic load conditions benefits from robust control to prevent performance degradation.

In this instance, the simulation time was set to 50 seconds. For the first simulation, the load torque is selected as follows:

$$T_L = \begin{cases} 0, & t \leq 10 \\ 0.15, & 10 < t \leq 30 \\ 0.3, & t > 30 \end{cases}$$

Figure 9 illustrates the variations in synchronization errors over time when a constant load is applied to the system. The results demonstrate that the proposed controller maintains effective performance even in the presence of the load.
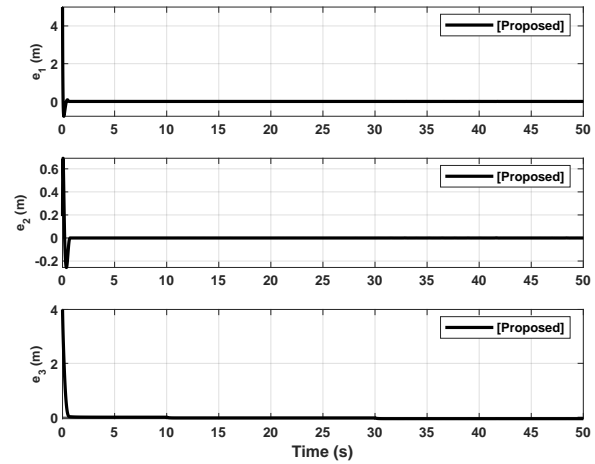

Fig. 9. Synchronization errors under constant load.

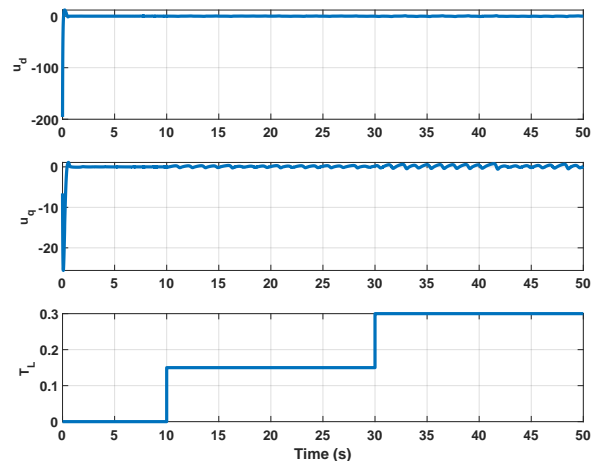Figure 10 presents the variations in control inputs and load torque applied to the system over time.

Fig. 10. Control inputs and values of constant load.

In an additional simulation, the load torque is specified as follows:

$$T_L = \begin{cases} 0, & t \leq 10 \\ 0.5\,(\sin t), & 10 < t \leq 30 \\ 0.15, & t > 30 \end{cases}$$

Figure 11 depicts the variations in synchronization errors over time for the simulation that considers both constant and variable load torque conditions. In this case, it is evident that the proposed control structure enables the system's errors to converge rapidly to a value near zero successfully.
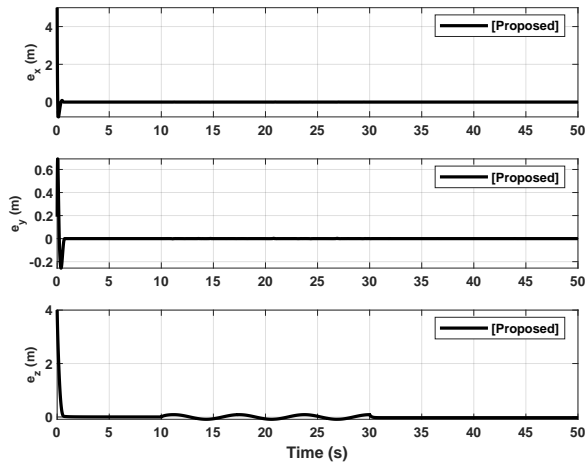
Fig. 11. Synchronization errors under constant and variable load.

Figure 12 illustrates the variations in control signals over time for the proposed controller, under the influence of both constant and variable load conditions.
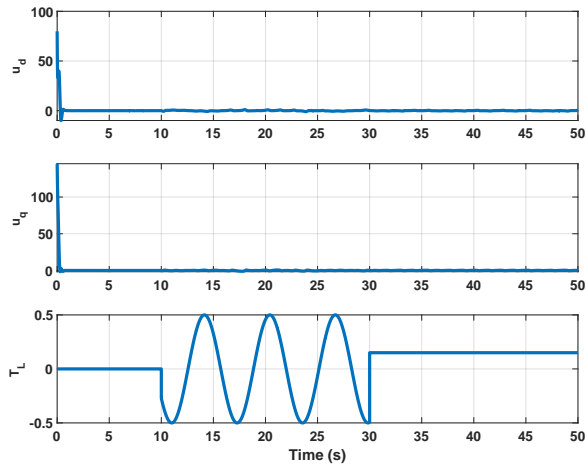

Fig. 12. Control inputs and values of constant and variable load.

Case 4: Different initial conditions

In the fourth scenario, it is demonstrated that the proposed control structure ensures the synchronization errors converge to a neighborhood close to zero, regardless of the initial conditions. Demonstrating robust performance under a variety of initial conditions is critical for systems that start from arbitrary states, for example, in fault recovery systems, where motors must restart smoothly after a fault or shutdown, regardless of the initial conditions. Additionally, in aerospace applications, satellite attitude control systems often require stabilization from varying initial orientations.

To evaluate this, three different initial conditions were selected for states $x_1(0), x_2(0), x_3(0), y_1(0), y_2(0), y_3(0)$ respectively as: IC1 = $[20, 0.01, -5, 25, 0.2, 1]$, IC2 = $[-3, 4, 12, 3, -8, 2]$, IC3 = $[5, 1, 5, 2.5, -3, 1]$ and the controller's performance was observed accordingly.

Figure 13 illustrates the time variations of synchronization errors under different initial conditions for the fractional-order

chaotic PMSM system controlled by the proposed controller. As observed in the figure, the proposed adaptive fractional order fixed-time sliding mode controller ensures that the synchronization errors converge to zero, irrespective of the initial conditions.
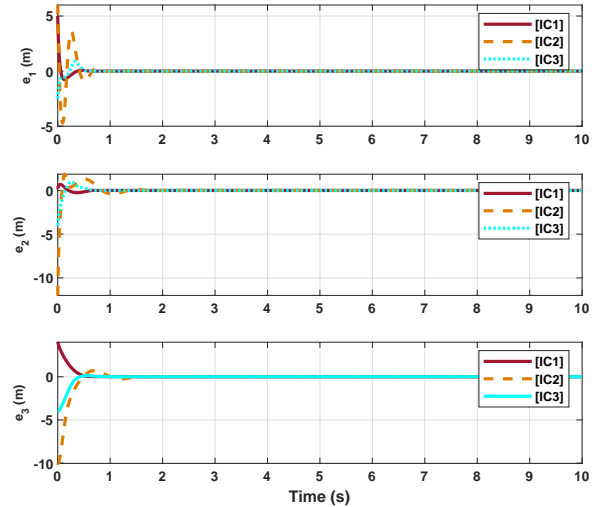

Fig. 13. Synchronization errors for different initial conditions.

Case 5: Disturbances and sensor noise

In the final scenario, to demonstrate the robustness of the proposed controller, simulations are performed by adding external disturbances and sensor noise to the system dynamics. The inclusion of disturbances and sensor noise addresses the unpredictability of real-world environments. Practical applications include autonomous vehicles, where sensor noise and environmental disturbances are prevalent, and the robustness of the controller ensures stable motor operation for navigation and propulsion. Also, in systems such as robotic surgical tools, the ability to operate effectively under noisy sensor data is critical for precision and safety.

The disturbances are modeled as: $d_i = 0.5\sin(t)$ with $i = 1, 2, 3$ and for the sensor noise, Gaussian noises are added to the states. Figure 14 shows how the master system's states change without controller when there are sensor noises.

Figure 15 shows the changes in system states over time when chaotic synchronization is performed with the proposed controller structure. As can be seen from the figure, the slave system successfully synchronizes with the master system using the proposed controller when considering external disturbances and sensor noise.

The changes in synchronization errors over time for the simulation that takes into account both disturbances and sensor noise are shown in Figure 16. Here, it is clear that the suggested control structure makes it possible for the system's errors to successfully converge quickly to a range close to zero.

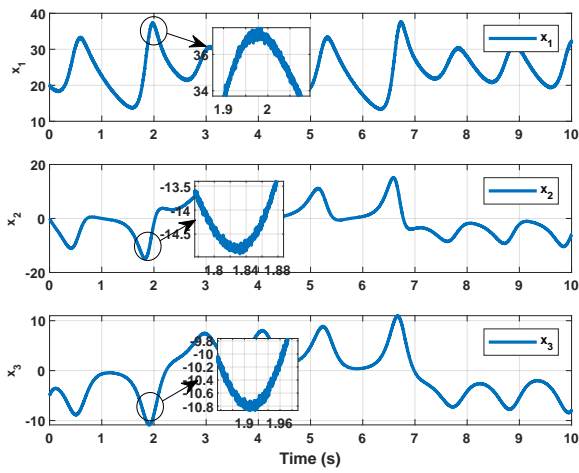Figure 17 shows the control input variations for the proposed controller.

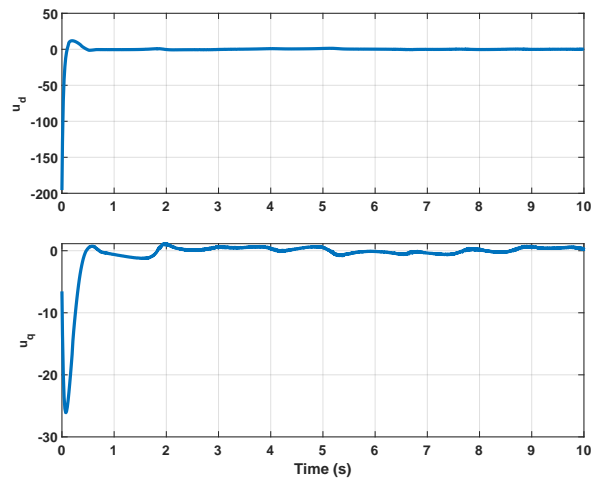Fig. 14.   States of master system under sensor noise without control.

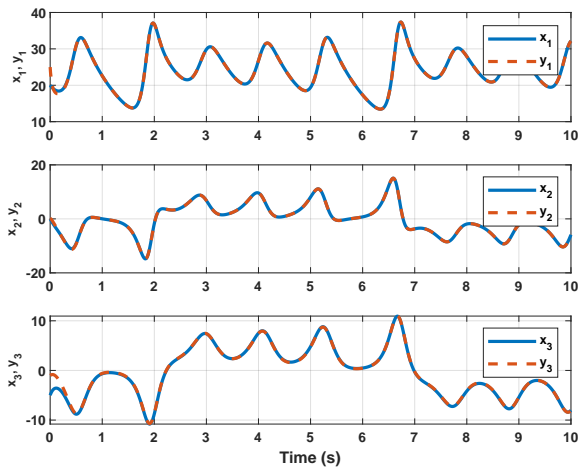Fig. 15.   System states for synchronization with disturbances and sensor noise.

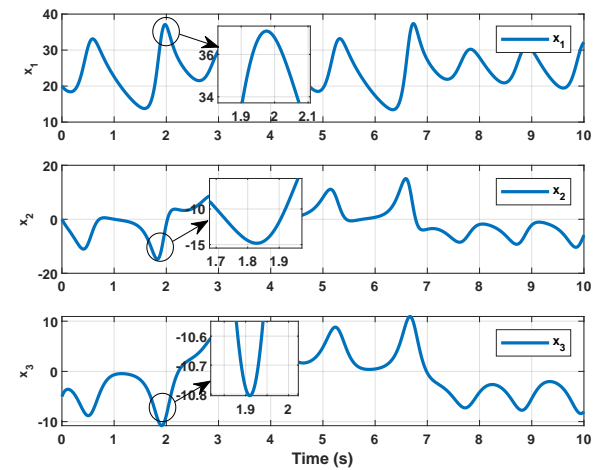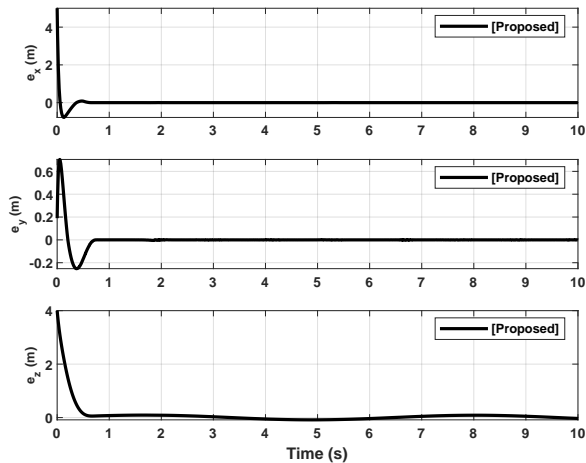Fig. 16.   Synchronization errors with disturbances and sensor noise.

Finally, Figure 18 illustrates how the master system's states change using the suggested controller during sensor noises. When compared to the case where the controller is not considered in Figure 14, it can be seen that the proposed control structure successfully eliminates the sensor noise.

Fig. 17.   Control inputs for synchronization with disturbances and sensor noise.

Fig. 18.   States of master system under sensor noise with control.

V. CONCLUSION

This study proposes a novel fractional-order adaptive fixed-time sliding mode controller for chaos suppression and synchronization in PMSMs. The controller integrates fractional calculus with fixed-time control theory to achieve robust performance, faster convergence, and reduced chattering compared to conventional methods. By incorporating an adaptive mechanism, the proposed controller dynamically adjusts its parameters to handle system uncertainties, external disturbances, and varying load conditions, ensuring stability and reliability under diverse scenarios. Simulation results demonstrate the controller's superior performance across various conditions, including synchronization, load variability, and diverse initial states. The results confirm fixed-time convergence, robustness to parameter variations, and effective handling of chaotic dynamics. The proposed method outperforms existing approaches in terms of settling time, robustness, and chattering reduction, as evidenced by quantitative comparisons. However, the study relies entirely on simulations, and several practical considerations, such as sensor noise, actuator delays, and hardware constraints, remain unaddressed. To bridge this gap

and enhance the practical applicability of the proposed controller, the following future works are planned: Experimental Validation: The controller will be implemented and tested on a laboratory-scale PMSM setup or through hardware-in-the-loop (HIL) platforms such as dSPACE or OPAL-RT to validate its performance under real-world conditions. Incorporation of Practical Constraints: Future studies will evaluate the controller's robustness to sensor noise, actuator delays, and hardware limitations, including computational delays and limited processing power in embedded systems. Strategies for addressing these challenges, such as simplified or predictive control designs, will be explored. Extension to Multi-Motor Systems: The controller will be adapted and tested for multi-motor synchronization and control scenarios, which are critical in robotics and industrial automation. Application-Specific Customization: The proposed method will be tailored and applied to specific domains, including electric vehicles, renewable energy systems, and robotics, where chaos suppression and precise synchronization are essential.

The promising results of this study, combined with the outlined future directions, indicate the potential of the proposed controller to significantly enhance the performance and stability of PMSMs in practical applications.

REFERENCES

[1] S. Lu and X. Wang, "Observer-based command filtered adaptive neural network tracking control for fractional-order chaotic pmsm," *IEEE Access*, vol. 7, pp. 88 777–88 788, 2019.

[2] D.-K. Hong, W. Hwang, J.-Y. Lee, and B.-C. Woo, "Design, analysis, and experimental validation of a permanent magnet synchronous motor for articulated robot applications," *IEEE Transactions on Magnetics*, vol. 54, no. 3, pp. 1–4, 2017.

[3] Z. Zhang, Q. Sun, and Q. Zhang, "A computationally efficient model predictive control method for dual three-phase pmsm of electric vehicle with fixed switching frequency," *IEEE Transactions on Industry Applications*, vol. 60, no. 1, pp. 1105–1116, 2023.

[4] J. Xu, B. Zhang, X. Kuang, H. Guo, and S. Guo, "Influence analysis of slot parameters and high torque density optimisation for dual redundant permanent magnet motor in aerospace application," *IET Electric Power Applications*, vol. 14, no. 7, pp. 1263–1273, 2020.

[5] Z. Maheshwari, K. Kengne, and O. Bhat, "A comprehensive review on wind turbine emulators," *Renewable and Sustainable Energy Reviews*, vol. 180, p. 113297, 2023.

[6] W. Xue, Y. Li, S. Cang, H. Jia, and Z. Wang, "Chaotic behavior and circuit implementation of a fractional-order permanent magnet synchronous motor model," *Journal of the franklin institute*, vol. 352, no. 7, pp. 2887–2898, 2015.

[7] M. Zribi, A. Oteafy, and N. Smaoui, "Controlling chaos in the permanent magnet synchronous motor," *Chaos, Solitons & Fractals*, vol. 41, no. 3, pp. 1266–1276, 2009.

[8] Y. Yu, X. Guo, and Z. Mi, "Adaptive robust backstepping control of permanent magnet synchronous motor chaotic system with fully unknown parameters and external disturbances," *Mathematical Problems in Engineering*, vol. 2016, no. 1, p. 3690240, 2016.

[9] J. Hu, Y. Qiu, and H. Lu, "Adaptive robust nonlinear feedback control of chaos in pmsm system with modeling uncertainty," *Applied Mathematical Modelling*, vol. 40, no. 19-20, pp. 8265–8275, 2016.

[10] Y. Song, Y. Tuo, and J. Li, "A neural adaptive prescribed performance controller for the chaotic pmsm stochastic system," *Nonlinear Dynamics*, vol. 111, no. 16, pp. 15 055–15 073, 2023.

[11] F. N. Deniz and M. Günay, "Coefficient diagram method based decentralized controller for fractional order tito systems," *Balkan Journal of Electrical and Computer Engineering*, vol. 10, no. 2, pp. 198–208, 2022.

[12] İ. E. Saçu, "Fractional integration based feature extractor for emg signals," *Balkan Journal of Electrical and Computer Engineering*, vol. 10, no. 2, pp. 132–138, 2022.

[13] C.-L. Li, S.-M. Yu, and X.-S. Luo, "Fractional-order permanent magnet synchronous motor and its adaptive chaotic control," *Chinese Physics B*, vol. 21, no. 10, p. 100506, 2012.

[14] L. Liu, D. Liang, C. Liu, and Q. Zhang, "Nonlinear state observer design for projective synchronization of fractional-order permanent magnet synchronous motor," *International Journal of Modern Physics B*, vol. 26, no. 30, p. 1250166, 2012.

[15] Y.-Y. Hou, A.-P. Lin, B.-W. Huang, C.-Y. Chen, M.-H. Lin, and H. Saberi-Nik, "On the dynamical behaviors in fractional-order complex pmsm system and hamilton energy control," *Nonlinear Dynamics*, vol. 112, no. 3, pp. 1861–1881, 2024.

[16] S. Lu, X. Wang, and L. Wang, "Finite-time adaptive neural network control for fractional-order chaotic pmsm via command filtered backstepping," *Advances in Difference Equations*, vol. 2020, no. 1, p. 121, 2020.

[17] Z. Zhan, X. Zhao, and R. Yang, "Recurrent neural networks with finite-time terminal sliding mode control for the fractional-order chaotic system with gaussian noise," *Indian Journal of Physics*, vol. 98, no. 1, pp. 291–300, 2024.

[18] A. Polyakov, "Nonlinear feedback design for fixed-time stabilization of linear control systems," *IEEE transactions on Automatic Control*, vol. 57, no. 8, pp. 2106–2110, 2011.

[19] M. Shirkavand, M. Pourgholi, and A. Yazdizadeh, "Robust global fixed-time synchronization of different dimensions fractional-order chaotic systems," *Chaos, Solitons & Fractals*, vol. 154, p. 111616, 2022.

[20] Y. Ai and H. Wang, "Fixed-time anti-synchronization of unified chaotic systems via adaptive backstepping approach," *IEEE Transactions on Circuits and Systems II: Express Briefs*, vol. 70, no. 2, pp. 626–630, 2022.

[21] H. Su, R. Luo, J. Fu, and M. Huang, "Fixed time control and synchronization of a class of uncertain chaotic systems with disturbances via passive control method," *Mathematics and Computers in Simulation*, vol. 198, pp. 474–493, 2022.

[22] M. J. Mirzaei, E. Aslmostafa, M. Asadollahi, and N. Padar, "Fast fixed-time sliding mode control for synchronization of chaotic systems with unmodeled dynamics and disturbance; applied to memristor-based oscillator," *Journal of Vibration and Control*, vol. 29, no. 9-10, pp. 2129–2143, 2023.

[23] F. W. Alsaade, Q. Yao, S. Bekiros, M. S. Al-zahrani, A. S. Alzahrani, and H. Jahanshahi, "Chaotic attitude synchronization and anti-synchronization of master-slave satellites using a robust fixed-time adaptive controller," *Chaos, Solitons & Fractals*, vol. 165, p. 112883, 2022.

[24] R.-R. Ma, Z. Huang, and H. Xu, "Fixed-time chaotic stabilization and synchronization of memristor chaotic circuits in noisy environments," *Journal of the Korean Physical Society*, vol. 84, no. 2, pp. 90–101, 2024.

[25] Z. Li, J. B. Park, Y. H. Joo, B. Zhang, and G. Chen, "Bifurcations and chaos in a permanent-magnet synchronous motor," *IEEE Transactions on Circuits and Systems I: Fundamental Theory and Applications*, vol. 49, no. 3, pp. 383–387, 2002.

[26] D. Xue, "Fotf toolbox for fractional-order control systems," *Applications in control*, vol. 6, pp. 237–266, 2019.

[27] K. Shao and X. Huang, "Finite-time synchronization of fractional-order pmsm with unknown parameters," in *2021 33rd Chinese Control and Decision Conference (CCDC)*.   IEEE, 2021, pp. 6234–6238.

Özhan Bingöl completed his undergraduate education in Electrical and Electronics Engineering at Firat University in 2012. He obtained his master's and doctoral degrees in the same field from Erzurum Technical University in 2019 and 2023, respectively. Since 2015, he has been serving as an academic at Gumushane University, within the Faculty of Engineering and Natural Sciences. He continues to conduct academic research in the area of control theory and its applications.